



Design and synthesis of *N*-hydroxyalkyl substituted deferiprone: a kind of iron chelating agents for Parkinson's disease chelation therapy strategy

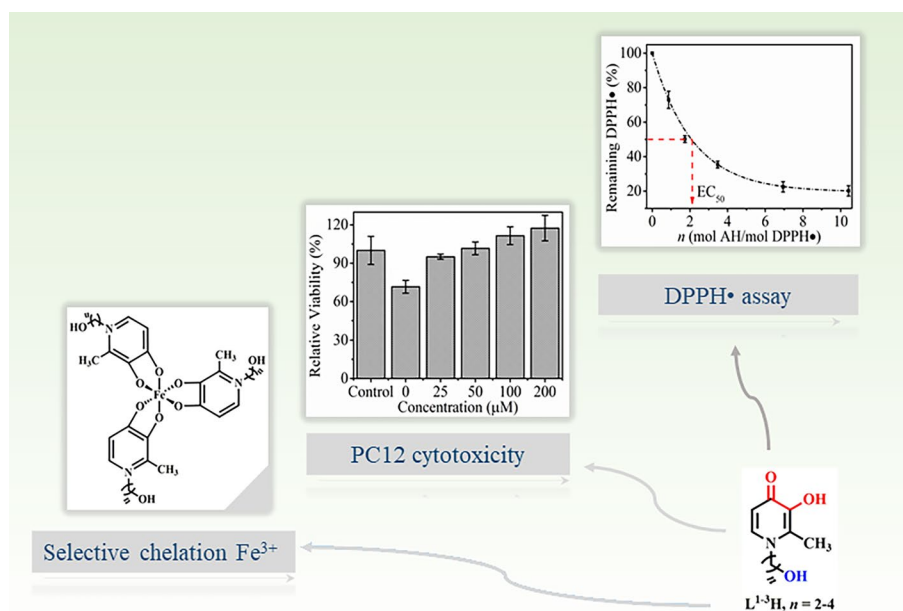
Qingchun Zhang¹ · Shufan Feng¹ · Yulian Zhao² · Bo Jin¹ · Rufang Peng¹

Received: 13 October 2020 / Accepted: 16 March 2021 / Published online: 8 May 2021
© Society for Biological Inorganic Chemistry (SBIC) 2021

Abstract

The blood–brain barrier (BBB) permeability of molecules needs to meet stringent requirements of Lipinski's rule, which pose a difficulty for the rational design of efficient chelating agents for Parkinson's disease chelation therapy. Therefore, the iron chelators employed *N*-aliphatic alcohols modification of deferiprone were reasonably designed in this work. The chelators not only meet Lipinski's rule for BBB permeability, but also ensure the iron affinity. The results of solution thermodynamics demonstrated that the $pK_{Fe^{3+}}$ value of *N*-hydroxyalkyl substituted deferiprone is between 19.20 and 19.36, which is comparable to that of clinical deferiprone. The results of 2,2-diphenyl-1-picrylhydrazyl radical scavenging assays indicated that the *N*-hydroxyalkyl substituted deferiprone also possesses similar radical scavenging ability in comparison to deferiprone. Meanwhile, the Cell Counting Kit-8 assays of neuron-like rat pheochromocytoma cell-line demonstrated that the *N*-hydroxyalkyl substituted deferiprone exhibits extremely low cytotoxicity and excellent H_2O_2 -induced oxidative stress protection effect. These results indicated that *N*-hydroxyalkyl substituted deferiprone has potential application prospects as chelating agents for Parkinson's disease chelation therapy strategy.

Graphic abstract



Keywords Hydroxypyridinone · Chelating agents · Deferiprone · Cytotoxicity · Solution thermodynamics · Parkinson's disease

Introduction

Iron is an essential cofactor for many proteins that are involved in the normal function of neuronal tissue, such as the non-haem iron enzyme tyrosine hydroxylase, which is required for dopamine synthesis. However, it has also become apparent that iron progressively accumulates in the brain with age, and that the redox cycle of ferric/ferrous valence states contributes to the enhanced generation of H_2O_2 , hydroxyl radicals, and other reactive oxygen species (ROSs), which can attack nigral dopaminergic neurons and induce neurodegeneration [1–5], and thereby induce neurodegenerative Parkinson's disease (PD). Therefore, the development of iron chelators that can mobilize iron out of the brain and eliminate the ROSs is generally considered to be a promising therapeutic strategy for disease mitigation [6–11].

However, the most important factor limiting the development of new iron chelators for the central nervous system (CNS) is the blood–brain barrier (BBB). The chelators cross the BBB via lipid-mediated free diffusion. According to Lipinski's rule, if the molecular weight of the drugs is greater than 500 Da and the calculated logarithm of partition coefficient ($\log P$) is greater than 5, or possess more than 5

H-bond donors, or possess more than 10 H-bond acceptors, the BBB permeability of the drugs does not increase in proportion to lipid solubility, then the drugs are probably poor BBB-penetrating molecules [12]. The BBB limits the brain penetration of essentially 100% of large-molecular drugs and more than 98% of small-molecular drugs [13, 14]. Considering that the number of individuals with a CNS condition will grow with an aging population, few satisfactory iron chelators become particularly problematic. Therefore, we urgently needed to develop iron chelators for PD chelation therapy.

In the past, chelation therapy has long been successfully used in treating beta-thalassemia, and then interest in the use of chelators as a therapeutic strategy in neurodegenerative disorders. But so far, only three iron chelators, deferiprone, deferasirox, and desferrioxamine (Fig. 1a), have been approved for clinical use in the chelation treatment of beta-thalassemia. Among them, only deferiprone has oral activity and BBB permeability, which have been employed in clinical studies for PD chelation therapy [15]. However, deferiprone is rapidly metabolized into non-chelating deferiprone 3-*O*-glucuronide by UDP-glucuronosyltransferases (UGTs, Fig. 1b) [16, 17], which leads to relatively high doses of deferiprone ($75 - 100 \text{ mg kg}^{-1}$) being adopted in

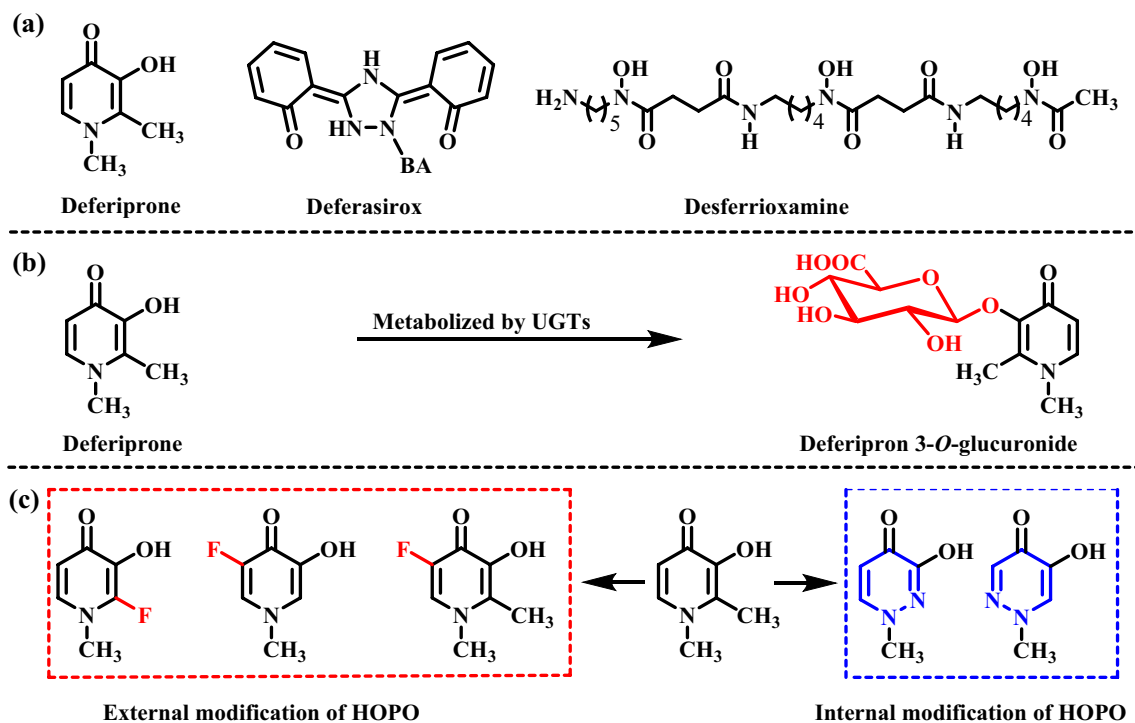


Fig. 1 a The molecular structures of three clinical use iron chelators. b The glucuronidation reaction of deferiprone. c The external and internal modification of HOPO

the clinic. In the case of considering Lipinski's rule [12] for BBB permeability, there have been several attempts to modify the deferiprone structure for optimizing the rate of metabolism. Such as internal and external modification of hydroxypyridinone (HOPO) ring (Fig. 1c). However, the introduction of additional nitrogen in or fluorine on HOPO ring [18, 19] significantly reduced iron affinity in comparison with deferiprone [19, 20]. Fortunately, the *N*-substituted modification of deferiprone has little effect on iron affinity [21–24]. Meanwhile, aliphatic alcohols could be glucuronidated by UGTs [25] and expected to reduce the rate of metabolism to non-chelating deferiprone 3-*O*-glucuronide. Therefore, the iron chelators employed *N*-aliphatic alcohols modification of deferiprone were reasonably designed in this work, which not only meet Lipinski's rule for BBB permeability and ensure iron affinity, but also may reduce the rate of deferiprone metabolism to non-chelating deferiprone 3-*O*-glucuronide. In consideration of the importance of Ca^{2+} and Zn^{2+} in organisms, the affinity of *N*-hydroxyalkyl substituted deferiprone with Ca^{2+} and Zn^{2+} also be studied.

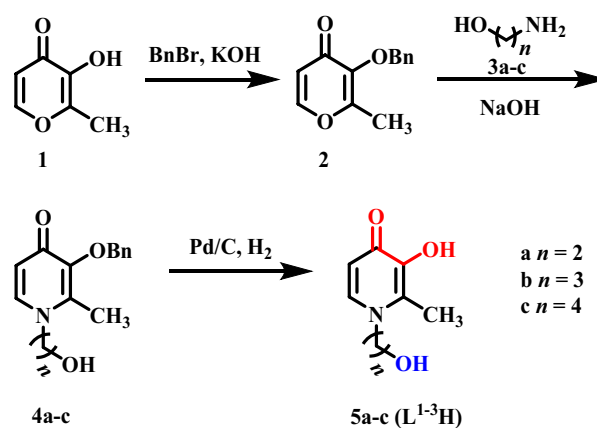
To the best of our knowledge, the radical scavenging activity and thermodynamic stability consequences of Fe^{3+} , Ca^{2+} and Zn^{2+} chelation by synthetic *N*-hydroxyalkyl substituted deferiprone chelators are as yet unexplored. Herein, the detailed characterization of the solution thermodynamic stability with Fe^{3+} , Ca^{2+} and Zn^{2+} , the radical scavenging activity, the cytotoxicity, and the H_2O_2 -induced oxidative stress protective effect of *N*-hydroxyalkyl substituted deferiprone are also discussed.

Results and discussion

Synthesis and characterization

The synthesis of *N*-hydroxyalkyl substituted deferiprone chelators **5a–c** (also designated as L^{1-3}H , due to their neutral form involved one dissociable proton) was shown in Scheme 1. 3-benzyloxy-2-methyl-4-pyrone **2** was prepared according to a universal hydroxyl protection method by using benzyl bromide. Alkanolamine **3a–c** and **2** were condensed using NaOH to obtain the desired pyridones **4a–c** with up to 82% yield [26]. Deprotection of the hydroxyl groups under typical catalytic hydrogenation conditions with the removal of the benzyl group gave the target product chelators L^{1-3}H up to 90% yield.

The chelators L^{1-3}H were fully characterized by nuclear magnetic resonance (NMR), Fourier-transform infrared (FTIR) spectroscopy, and mass spectra (MS). The FTIR spectra of chelators L^{1-3}H showed characteristic peaks at about 3304 cm^{-1} for $\nu(\text{O}-\text{H})$ of the HOPO hydroxy group, 1622 cm^{-1} for $\nu(\text{C}=\text{O})$ of HOPO carbonyl, and 1562 cm^{-1} , 1499 cm^{-1} for pyridone ring skeleton vibration.



Scheme 1 Synthesis of *N*-hydroxyalkyl substituted deferiprone chelators. Metal-binding atoms are shown in red, and aliphatic alcohol that can be glucuronidated by UGTs is shown in blue

The ^1H NMR signals of the HOPO protons of chelators L^{1-3}H in D_2O were identified as two doublets at 7.65 ppm (d, $J=7.2$ Hz, 1H, Py-*H*) and 6.52 ppm (d, $J=7.2$ Hz, 1H, Py-*H*). The results indicated that the structures of chelators L^{1-3}H were as we expected.

Solution thermodynamics

In the presence of dissolved metal ions (M^{a+}) and protonated chelators (LH_h , where L is a ligand with h removable protons), a pH-dependent metal–ligand complex with the general formula $\text{M}_m\text{L}_l\text{H}_h$ forms. The relative amount of each species in solution was determined by Eq. 1, whose rearrangement provides the standard formation constant notation of $\log \beta_{mlh}$ (Eq. 2). The $\log \beta_{mlh}$ value describes a cumulative formation constant, and a stepwise formation constant ($\log K$) can be calculated from $\log \beta_{mlh}$ value by using Eq. 3. When addressing protonation constants, the stepwise formation constants are commonly reported as $\log K_h^{\text{H}}$.

$$[\text{M}_m\text{L}_l\text{H}_h] = \beta_{mlh} [\text{M}]^m [\text{L}]^l [\text{H}]^h \quad (1)$$

$$\log \beta_{mlh} = \log \left(\frac{[\text{M}_m\text{L}_l\text{H}_h]}{[\text{M}]^m [\text{L}]^l [\text{H}]^h} \right) \quad (2)$$

$$\log K_{01h} = \log \left(\frac{[\text{LH}_h]}{[\text{LH}_{h-1}] [\text{H}]} \right) = \log \left(\frac{\beta_{01h}}{\beta_{01(h-1)}} \right) \quad (3)$$

Protonation of chelators L^{1-3}H

Before studying the complexation of metal ions by the investigated chelators L^{1-3}H , the $\log K_h^{\text{H}}$ value of chelators L^{1-3}H should be determined. The $\log K_h^{\text{H}}$ value of chelators L^{1-3}H

Fig. 2 Incremental spectrophotometric titration of chelator L^1H **a** by 0.1 M HNO_3 , **b** by 0.1 M KOH . Conditions: $[L^1H]=0.2$ mM, $I=0.1$ M KCl , $T=298$ K

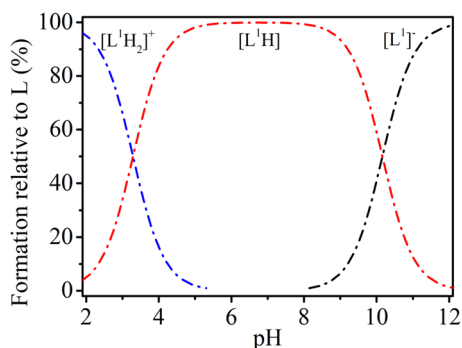
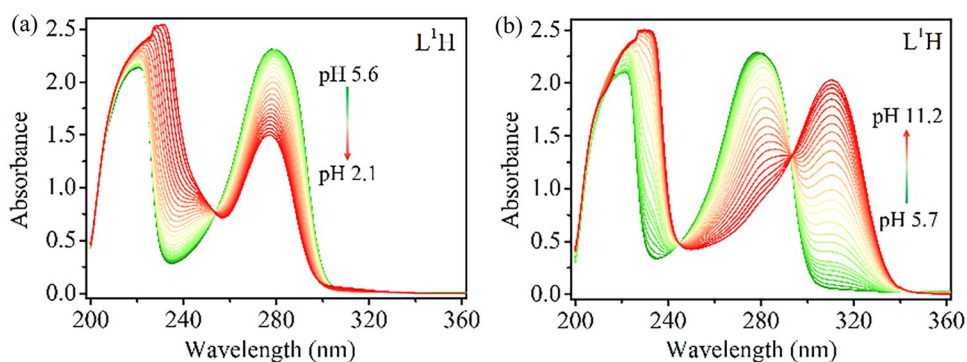


Fig. 3 Representative speciation diagram of chelator L^1H calculated at concentration of $10 \mu M$

was calculated by program HypSpec [27], fitting incremental spectrophotometric titration data. In their neutral form, the initial intensity of peaks at 280 nm gradually decreases with a decrease in pH in the range 5.6–2.1, which was attributed to the protonation of the carbonyl group. And the initial maximum UV–visible absorption peaks at 280 nm redshift to 310 nm with an increase in pH in the range 5.7–11.2, which was attributed to the deprotonation of the hydroxyl of HOPO (Fig. 2 and Figures S1–S2). The $\log K_h^H$ value was used to calculate the speciation diagram by program HySS [28] and three different species obtained between pH 2.0 and 12.0 (Fig. 3 and Figure S3). To determine the accuracy of the results, the $\log K_h^H$ value of chelators $L^{1-3}H$ was confirmed by program HyperQuad [29] fitting potentiometric titration curves (Figure S4). The curves of free chelators $L^{1-3}H$ all show a break at $m=0$ (mol base/mol chelator) and low pH value ($pH < 9.0$), which is indicative of the deprotonation of the hydroxyl of HOPO. The $\log K_h^H$ value extrapolated from both methods was in excellent agreement (Figure S5). The determined $\log K_h^H$ value of chelators $L^{1-3}H$ is listed in Table 1. The $\log K_1^H$ value of chelators $L^{1-3}H$, corresponding to the first protonation of the stronger basic oxygen atoms of the HOPO anion moiety (Scheme 2), is in good agreement with the reported value of $\log K_1^H=9.82$ for deferiprone [30] (Table 1). The $\log K_2^H$ value of chelators

Table 1 Summary of $\log K_h^H$ value of chelators $L^{1-3}H$ and deferiprone

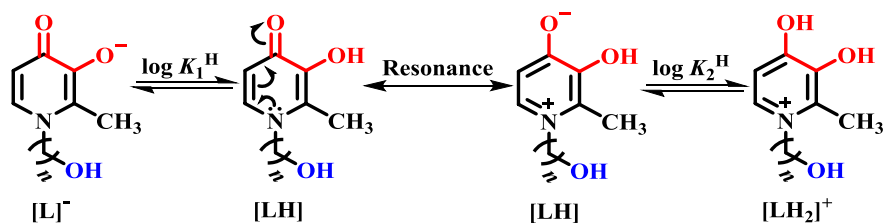
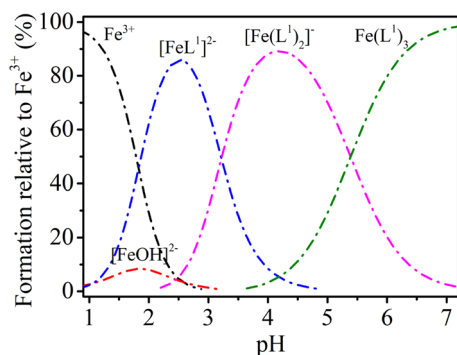
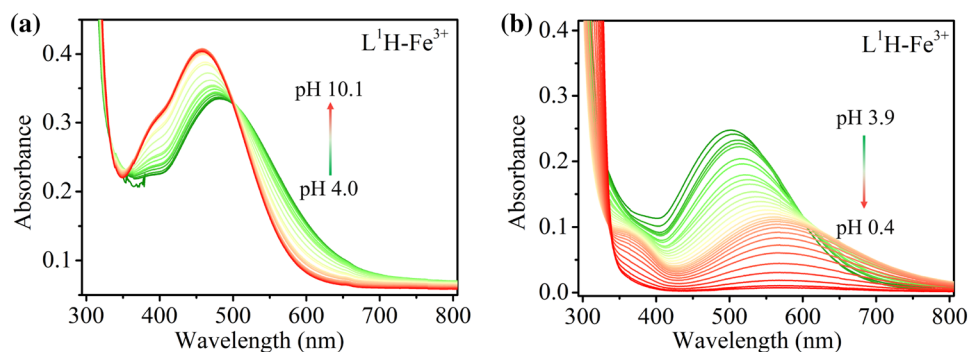
Chelator	$\log K_1^H$	$\log K_2^H$
L^1H^a	10.16 (3)	3.29 (2)
L^2H^a	10.01 (4)	3.34 (2)
L^3H^a	9.98 (2)	3.22 (3)
Deferiprone ^b	9.82	3.66

^aValue was determined from incremental spectrophotometric titrations at $[L^{1-3}H]=0.2$ mM, $I=0.1$ M KCl , $T=298$ K. ^bValue was obtained from Ref. [30] at [deferiprone]=0.32 mM, $I=0.1$ M KCl , $T=298$ K

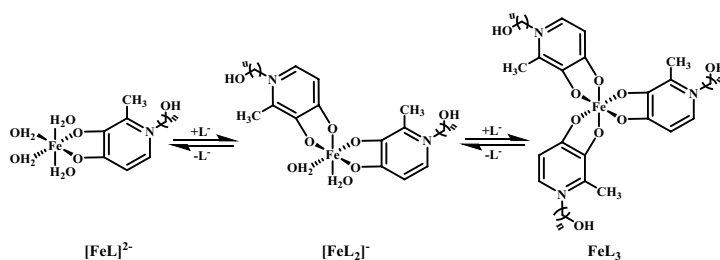
$L^{1-3}H$ is ascribed to the protonation of carbonylic oxygen of the HOPO moiety (Scheme 2). The value is slightly lower than that of deferiprone [30] (Table 1), which is attributed to the intermolecular hydrogen bond between aliphatic alcohol and carbonyl that makes carbonyl difficult to protonate.

Iron(III) complexation

The affinities of chelators $L^{1-3}H$ with Fe^{3+} were determined by incremental spectrophotometric titrations using a 1:3 Fe^{3+} to chelator ratio to ensure the formation of mononuclear complexes. Compared with the free chelators, the UV–visible of complexes $Fe^{3+} - L^{1-3}H$ have new absorption peaks at wavelengths greater than 400 nm. The absorption peaks at about 580 nm blue-shift to about 460 nm with an increase in pH in the range 0.4–10.1, were attributed to the ligand to metal charge transfer (LMCT) peaks of complexes $Fe^{3+} - L^{1-3}H$ (Fig. 4 and Figure S6–S7). In the UV–visible spectra, the LMCT peaks can be assigned to three spectrophotometrically distinguishable species of complexes, which were used to determine the $\log \beta_{mlh}$ value. The $Fe^{3+} - L^{1-3}H$ complexes routinely form $[FeL^{1-3}]^{2-}$, which are generated at pH 1.0. The LMCT peaks at 580 nm gradually increase and blue-shift to about 500 nm with an increase in pH in the range of about 1.0–5.5, which indicated the deprotonation of another free chelator and complexation with

Scheme 2 Protonation process of chelators $L^{1-3}H$ **Fig. 4** Incremental spectrophotometric titration of the complex L^1H-Fe^{3+} **a** by 0.1 M KOH, **b** by 0.1 M HNO_3 . Conditions: $[L^1H] = 3 \times [Fe^{3+}] = 0.2$ mM, $I = 0.1$ M KCl, $T = 298$ K**Fig. 5** Representative speciation diagram of complex $Fe^{3+}-L^1H$ calculated at $[Fe^{3+}] = 1$ μ M and $[L^1H] = 10$ μ M

$[FeL^{1-3}]^{2-}$ continuing to generate $[Fe(L^{1-3})_2]^{-}$. Subsequently, the LMCT peaks at 500 nm further gradually increase and blue-shift to about 460 nm with an increase in pH in the range of about 5.5 – 7.0, which indicated the complete deprotonation of free chelators $L^{1-3}H$ and complexation with $[Fe(L^{1-3})_2]^{-}$ to generate $[Fe(L^{1-3})_3]$ (Fig. 5 and Figure S8). The complexation processes are proposed that complete deprotonation chelators $L^{1-3}H$ gradually

Scheme 3 Proposed complexation processes of chelators $L^{1-3}H$; the charge numbers are omitted for clarity

replaced water molecules coordinated with Fe^{3+} with an increase in pH value (Scheme 3).

The determined thermodynamic parameters of $Fe^{3+}-L^{1-3}H$ complexes and corresponding complexes of deferiprone are listed in Table 2. Because $\log \beta_{mlh}$ value is species-dependent, a species-independent metric is needed to compare affinities of various chelators with Fe^{3+} . In this regard, pM is the metric employed, where $pM = -\log[M_{free}]$. “ M_{free} ” refers to solvated metal ions free of complexation by chelators or hydroxides, with a high pM value corresponding to low concentrations of free metal ions in solution. In this study, pM value is calculated using standard conditions of $[M] = 1$ μ M and $[L^{1-3}H] = 10$ μ M at a typical pH of 7.4. The pFe^{3+} value of the chelators $L^{1-3}H$ is significantly higher than that of nitrogen internal modification of HOPO [19] and fluorine external modification of HOPO [19, 20], which are attributed to the more electronegative nitrogen atom replacing carbon atom in HOPO moiety and the negative inductive effect of fluorine on HOPO moiety, respectively. In comparison to deferiprone, the pFe^{3+} value of chelators $L^{1-3}H$ is slightly lower (Table 2) [30], which is attributed to the longer *N*-hydroxyalkyl substituent of chelators $L^{1-3}H$ leading to greater steric hindrance.

Table 2 Summary of the thermodynamic parameters of complexes $\text{Fe}^{3+} - \text{L}^{1-3}\text{H}$ and comparison with corresponding complexes of deferiprone

Chelator	$\log \beta_{110}$	$\log \beta_{120}$	$\log \beta_{130}$	$\text{pFe}^{3+ e}$
L^1H^a	14.83 (3)	27.18 (4)	37.08 (2)	19.36 (3)
L^2H^a	14.58 (3)	27.10 (3)	36.62 (3)	19.35 (3)
L^3H^a	14.50 (4)	27.07 (5)	36.44 (3)	19.20 (4)
3-hydroxy-1-methylpyridazin-4-one ^b	9.6	17.2	23.2	14.8
5-hydroxy-1-methylpyridazin-4-one ^b	10.2	19.3	26.8	17.2
5-fluoro-3-hydroxy-1-methyl-4(1H)-pyridone ^c	/	/	/	18.5
5-fluoro-3-hydroxy-1,2-dimethyl-4(1H)-pyridone ^c	/	/	/	18.5
deferiprone ^d	15.01	27.30	37.43	20.67

^aValue was determined from incremental spectrophotometric titrations at $[\text{L}^{1-3}\text{H}] = 3 \times [\text{Fe}^{3+}] = 0.2 \text{ mM}$, $I = 0.1 \text{ M KCl}$, $T = 298 \text{ K}$. ^bValue was obtained from Ref. [19]. ^cValue was obtained from Ref. [20]. ^dValue was obtained from Ref. [30] at $[\text{deferiprone}] = 3 \times [\text{Fe}^{3+}] = 0.75 \text{ mM}$, $I = 0.1 \text{ M KCl}$, $T = 298 \text{ K}$. ^e pFe^{3+} is the negative logarithm of the free Fe^{3+} concentration in equilibrium with complexed and free chelator at a fixed pH of 7.4 with $1 \mu\text{M}$ total Fe^{3+} concentration and $10 \mu\text{M}$ total chelator concentration

Calcium(II) and Zinc(II) complexation

The affinities of chelators L^{1-3}H with Ca^{2+} or Zn^{2+} were also determined by incremental spectrophotometric titrations using a 1:1 metal cation to chelator ratio.

The initial maximum UV – visible absorption peaks of complexes $\text{Ca}^{2+} - \text{L}^{1-3}\text{H}$ at 280 nm red-shift to 310 nm and the solution becomes cloudy with an increase in pH in the range about 5.7 – 11.2, which was attributed to the deprotonation of the hydroxyl of HOPO (Figure S9 – S11) and the hydrolysis of Ca^{2+} . The initial pH values of the solution of complexes $\text{Ca}^{2+} - \text{L}^{1-3}\text{H}$ compared to that of free chelators L^{1-3}H are almost unchanged. Meanwhile, the curves of absorbance at 280 nm and 310 nm of free chelators L^{1-3}H and complexes $\text{Ca}^{2+} - \text{L}^{1-3}\text{H}$ as a function of pH were almost overlapping (Figure S12), and the potentiometric titration curves of free chelators L^{1-3}H and complexes $\text{Ca}^{2+} - \text{L}^{1-3}\text{H}$ were also almost overlapping (Figure S4). The results indicated that the free chelators L^{1-3}H have been completely deprotonated, but not coordinated with Ca^{2+} to form complexes. Hence, the affinity of chelators L^{1-3}H with Ca^{2+} was negligible.

The initial maximum UV – visible absorption peaks of complexes $\text{Zn}^{2+} - \text{L}^{1-3}\text{H}$ at 280 nm also red-shift to 310 nm with an increase in pH in the range of about 5.2 – 10.2, which was attributed to the deprotonation of the hydroxyl of HOPO (Figure S13 – S15). The initial pH values of the solution of complexes $\text{Zn}^{2+} - \text{L}^{1-3}\text{H}$ compared to that of free chelators L^{1-3}H , have a significant decrease. The results indicated that the free chelators L^{1-3}H have a certain affinity for Zn^{2+} . Incremental spectrophotometric titrations were used to determine the $\log \beta_{mlh}$ value of complexes $\text{Zn}^{2+} - \text{L}^{1-3}\text{H}$, and variations in the UV – visible absorbance at varying pH were modeled by the formation of one distinguishable species between about pH 6.0 and 10.0 (Figure S16). The determined thermodynamic parameters of complexes $\text{Zn}^{2+} - \text{L}^{1-3}\text{H}$ and corresponding complexes of deferiprone

[26], 1,4,7,10-tetraazacyclododecane-*N,N',N'',N'''*-tetraacetic acid (DOTA) [31], and diethylenetriaminepentaacetic acid (DTPA) [32] are listed in Table 3. The pZn^{2+} value of chelators L^{1-3}H is significantly lower than those of the traditional chelators DOTA and DTPA, and also similar to deferiprone [26] and other HOPO chelators [33–35], indicating that chelators L^{1-3}H exhibited the poor affinity with Zn^{2+} .

The results of the above-mentioned solution thermodynamics demonstrated that the chelators L^{1-3}H have almost no chelating ability to important Ca^{2+} and Zn^{2+} in vivo, but have strong chelating ability to Fe^{3+} , the pFe^{3+} value up to 19.36, which indicated that the chelators L^{1-3}H exhibited selective chelating ability to Fe^{3+} .

Table 3 Summary of the thermodynamic parameters of complexes $\text{Zn}^{2+} - \text{L}^{1-3}\text{H}$ and comparison with corresponding complexes of deferiprone, DOTA, and DTPA

Chelator	$\log \beta_{110}$	$\text{pZn}^{2+ e}$
L^1H^a	7.08 (2)	6.08 (3)
L^2H^a	7.06 (3)	6.11 (4)
L^3H^a	7.02 (3)	6.10 (3)
Deferiprone ^b	7.19	6.20
DOTA ^c	21.10	17.90
DTPA ^d	17.45	14.80

^aValue was determined from incremental spectrophotometric titrations at $[\text{L}^{1-3}\text{H}] = [\text{Zn}^{2+}] = 0.2 \text{ mM}$, $I = 0.1 \text{ M KCl}$, $T = 298 \text{ K}$. ^bValue was obtained from Ref. [26] at $I = 0.1 \text{ M KNO}_3$, $T = 298 \text{ K}$. ^cValue was obtained from Ref. [31]. ^dValue was obtained from Ref. [32]. ^e pZn^{2+} is the negative logarithm of the free Zn^{2+} concentration in equilibrium with complexed and free chelator at a fixed pH of 7.4 with $1 \mu\text{M}$ total Zn^{2+} concentration and $10 \mu\text{M}$ total chelator concentration

Free radical scavenging activity

2,2-diphenyl-1-picrylhydrazyl (DPPH•) as stable free radical [36] has been widely used to monitor the free radical scavenging ability of antioxidants [37–39]. The assays were carried out in methanol, and the results are expressed as EC_{50} , which represents the antioxidant concentration required to decrease the initial DPPH• concentration by 50%. A low EC_{50} value indicates a high radical scavenging ability. The kinetics of the DPPH• reaction indicated that chelators $L^{1-3}H$ can be classified as slow reaction [40], and the reaction reached steady-state at least 3 h. The EC_{50} value of chelators $L^{1-3}H$ was obtained from the curves of the percentage of remaining DPPH• as a function of concentration n , where n is the molar ratio of antioxidant to DPPH•. The EC_{50} value of chelators $L^{1-3}H$ is between 2.00 and 2.11, which is slightly more than 1.86 of deferiprone (Figure S17 and Table S1). In polar methanol, the reaction between DPPH• and phenolic hydroxyl analogs dominated by an electron transfer mechanism. The process of electron transfer from phenolic hydroxyl analogs to DPPH• is very fast [41]. Therefore, the number of phenolic hydroxyl analogs determines the free radical scavenging ability [42]; the more the phenolic hydroxyl analogs, the better the performance [43]. The chelators $L^{1-3}H$, deferiprone, and butylated hydroxyanisole [44] possess analogue monophenolic structure, which leads them to approximate EC_{50} values (Table S1). In comparison with chelators $L^{1-3}H$, the catechol possesses more

phenolic hydroxyl leading to lower EC_{50} value. The results were as expected.

Cytotoxicity and H_2O_2 -induced oxidative stress protective effect

Cytotoxicity and H_2O_2 -induced oxidative stress protection effect of chelators $L^{1-3}H$ and deferiprone were evaluated by using neuron-like rat pheochromocytoma cell-line (PC12) in vitro, which was widely used to study neurodegenerative diseases [45]. The PC12 cells were incubated with the chelators $L^{1-3}H$ and deferiprone for 48 h under various concentrations, and then the Cell Counting Kit-8 (CCK-8) assays were performed to examine cytotoxicity. In comparison with a control group, the relative viability of PC12 cells incubation with chelators $L^{1-3}H$ increased slightly at all concentrations. Meanwhile, the relative viability of chelators $L^{1-3}H$ was comparable to that of clinical deferiprone (Fig. 6). The results concluded that the chelators $L^{1-3}H$ are non-toxic to PC12 cells. The PC12 cells were incubated with 100 μM H_2O_2 and various concentrations of chelators $L^{1-3}H$ and deferiprone for 48 h, and then the CCK-8 assays were performed to examine the H_2O_2 -induced oxidative stress protection effect. In comparison with the control group incubated with only 100 μM H_2O_2 , the relative viability increased significantly with the addition of chelators $L^{1-3}H$, which increased with the increase of concentration of chelators $L^{1-3}H$ (Fig. 7a–c). The results indicated that the chelators

Fig. 6 The relative viability of PC12 cell incubation with **a** chelator L^1H , **b** chelator L^2H , **c** chelator L^3H , and **d** deferiprone for 48 h under various concentrations. Value is reported as the mean \pm SD of three independent experiments

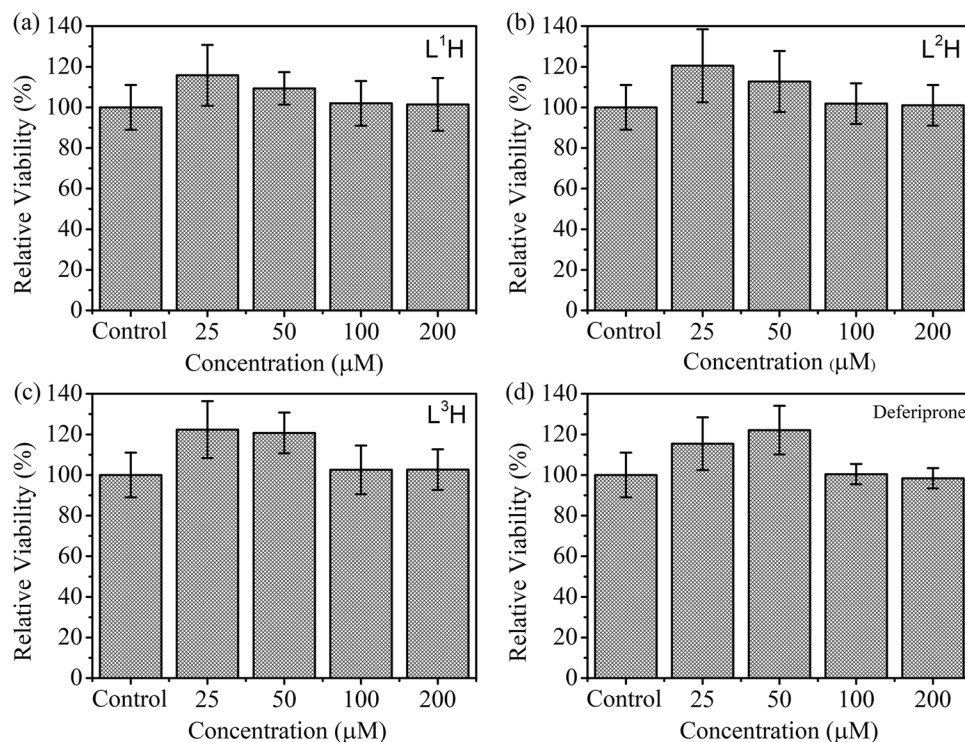
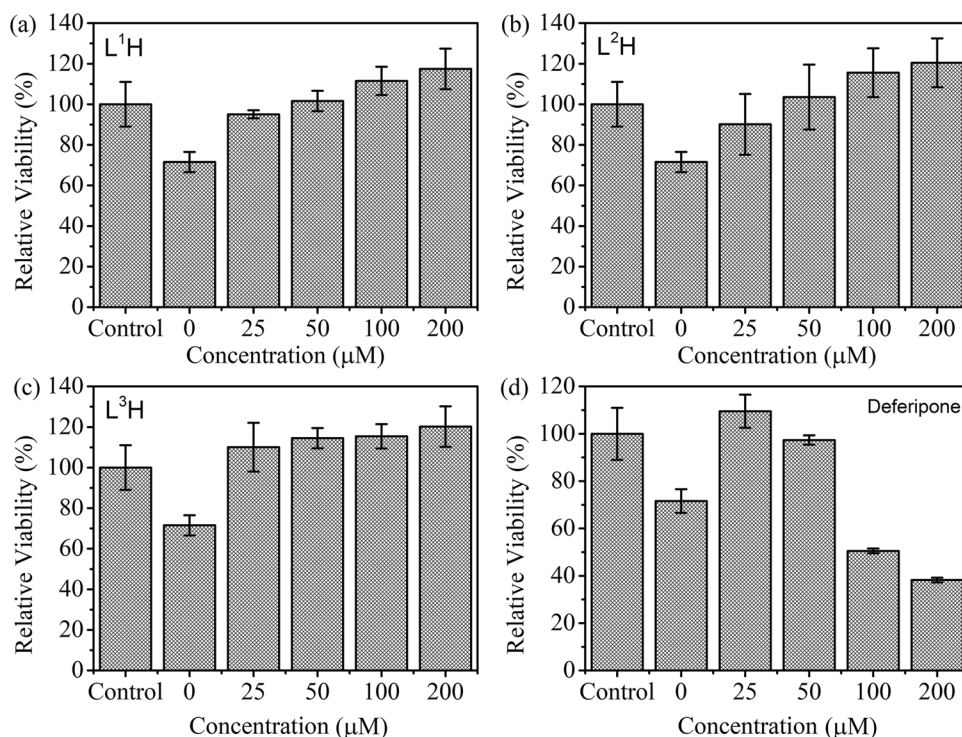


Fig. 7 The relative viability of PC12 cells incubation with 100 μM H_2O_2 and **a** chelator L^1H , **b** chelator L^2H , **c** chelator L^3H , **d** deferiprone for 48 h under various concentrations. Value is reported as the mean \pm SD of three independent experiments



L^{1-3}H protected PC12 cells against H_2O_2 -induced oxidative stress, and the antioxidative effect was significant. The PC12 cells' incubation with 100 μM H_2O_2 and various concentrations of deferiprone was also tested, and the relative viability was increased to about 110 and 97% at lower concentration 25 and 50 μM , respectively (Fig. 7d). But as the concentration increased, the relative viability rate quickly decreased to 38% at concentration of 200 μM (Fig. 7d), and no protective effect on H_2O_2 -induced oxidative stress was observed, which indicated a maximum dose threshold to the protective benefits of deferiprone.

BBB permeability

The chelators cross the BBB via lipid-mediated free diffusion in pharmacologically significant amounts, which is mainly controlled by molecular weight, lipophilicity, and net charge. These general parameters have been used by Lipinski [12] to predict BBB permeability. If the molecular weight of the drugs is lower than 500 Da and calculated $\log P$ is lower than 5, and the drugs possess less than 5 H-bond donors as well as less than 10 H-bond acceptors, the drugs are probably BBB-penetrating molecules. The four parameters of chelators L^{1-3}H are slightly higher than deferiprone, but in full compliance with Lipinski's rule (Table 4), indicated that chelators L^{1-3}H may have good permeability similar to deferiprone.

Table 4 Parameters of iron chelators for evaluating permeability according to Lipinski's rule

Chelator	Molecular weight	H bond donors	H bond acceptors	$\log P$
Lipinski's rule threshold	500	5	10	5
L^1H^a	169	2	4	-1.1
L^2H^a	183	2	4	-0.89
L^3H^a	197	2	4	-0.75
Deferiprone ^a	139	1	3	-0.77

^aThe $\log P$ value was obtained from Ref. [46] and determined by hand-shake method at *n*-octanol and water system, pH=7.4, $T=298\text{ K}$

Conclusions

A series of *N*-hydroxyalkyl substituted deferiprone chelators L^{1-3}H , which could be used for PD chelation therapy, have been synthesized. The results of solution thermodynamics demonstrated that the chelators L^{1-3}H have almost no chelating ability to important Ca^{2+} and Zn^{2+} , but have strong chelating ability to Fe^{3+} , the pFe^{3+} value as high as 19.36. It was concluded that the chelators L^{1-3}H exhibited selective chelating ability to Fe^{3+} . The results of DPPH• scavenging assays indicated that the chelators L^{1-3}H also exhibit similar radical scavenging ability in comparison to deferiprone. Meanwhile, the results of CCK-8 assays indicated that the chelators L^{1-3}H possessed extremely low

cytotoxicity and excellent H₂O₂-induced oxidative stress protection effect on PC12 cells. These results indicated that the chelators L^{1–3}H have potential application prospects as chelating agents for Parkinson's disease chelation therapy strategy.

Experimental section

Chelators and metal cations stock solutions

Aqueous stock solutions of chelators L^{1–3}H were freshly prepared by direct dissolution of a weighed amount of chelators in 0.1 M KCl aqueous solution before each set of experiments. A Fe³⁺ stock solution was prepared by dissolving a weighed amount of corresponding ferric nitrate (Fe(NO₃)₃·9H₂O, 99.99% metals basis) in ultrapure water and calibration by EDTA method to obtain 0.2 M stock solution. A Ca²⁺ and Zn²⁺ stock solution was prepared by dissolving a weighed amount of corresponding calcium chloride (CaCl₂·2H₂O, 99.9% metals basis) and (ZnCl₂·2H₂O, 99.9% metals basis) in ultrapure water to obtain 0.2 M stock solution. All solid reagents were weighed on a Sartorius BT25S analytical balance that was accurate to 0.01 mg. All titration solutions were prepared using distilled water from Ulupure ULUP-IV ultra water system and degassed by ultrasonic device.

Potentiometric titrations

Potentiometric titrations were carried out with INESA ZDJ-4B automated titrator. The solution was maintained at 298 K by an external thermostated water bath. The analyte solution was bubbled with N₂ gas in each set of experiments and measurement performed in 0.1 M KCl electrolyte to correct for the ionic strength. The pH electrode (INESA, equipped with a Metrohm combination electrode in saturated KCl) was calibrated to measure p[H] (hydrogen ion concentration) by standardized pH buffer (Hamilton). All analyte solutions were prepared in a 50.0 mL volumetric flask. The potential measurements were conducted with solution of a chelator to metal ratio of 3:1 for Fe³⁺ complexes and a chelator to metal ratio of 1:1 for Ca²⁺ and Zn²⁺ complexes by careful addition of the chelator stock solution, corresponding metal ion stock solution and 50.0 μL standardized 0.1 M HNO₃ solution. Titrations of free chelators and metal complexes used standardized 0.1 M KOH as the titrant (Aladdin). The potentiometric titration data were used in the Hyperquad refinements [29], and titrations were repeated a minimum of three times.

Spectrophotometric titrations

Spectrophotometric titrations were also carried out with INESA ZDJ-4B automated titrator. The solution was maintained at 298 K by an external thermostated water bath. All analyte solutions were prepared in a 50.0 mL volumetric flask. The measurements were conducted with a chelator to metal ratio of 3:1 for Fe³⁺ complexes and a chelator to metal ratio of 1:1 for Ca²⁺ and Zn²⁺ complexes by careful addition of the chelator stock solution and corresponding metal ion stock solution. Measurements of analyte solutions with different pHs were made on a Thermo Scientific Evolution 201 UV – vis spectrophotometer using a 10.0-mm quartz flow cell. The scan range of spectra was typically 200–360 nm, except the Fe³⁺ complexes were 300–800 nm. The stability constants and spectral deconvolution were refined using the least-squares fitting program HypSpec [27].

Titration data treatment

The potentiometric titration and spectrophotometric titration data were, respectively, analyzed by the programs Hyperquad [29] and HypSpec [27], utilizing nonlinear least-squares fitting to refine stability constants and protonation constants. The pM value and speciation diagrams were calculated by the program HySS [28] with protonation constants of chelators (Table 1), formation constants of metal complexes (Tables 2 and 3), metal cation hydrolysis stability constants, and water solubility product constant (Table S2). Errors were determined as $t^*s/(n)^{1/2}$ at the 95% probability level, where n is the number of samples, $s/(n)^{1/2}$ is the standard deviation, and t^* is the distribution over $n - 1$ degree of freedom. The errors quoted in Tables 1, 2 and 3 were used to account for error propagations, which are the standard deviations of the overall thermodynamic parameters given directly by the programs Hyperquad [29] and HypSpec [27] for the input potentiometric titration data and batch spectrophotometric titration data, which include the experimental points of all the titration data.

DPPH• scavenging assays

An aliquot of methanol (50.0 μL) and different aliquots of stock methanol solutions of 2.5 mM chelators were added to a 2.4-mL methanol solution of 0.06 mM DPPH•, and the volume was adjusted to a final value of 3.0 mL with methanol. Absorbances at 517 nm were measured on a Thermo Scientific Evolution 201 UV – vis spectrophotometer after the solution in a dark environment for 3 h until the reaction reached a steady state. Five different concentrations were measured for each assay, which was repeated a minimum of three times. Then the EC₅₀ value was plotted to obtain from the percentage of remaining.

Cells and culture conditions

The PC12 cells (iCell Bioscience Inc, Shanghai) were cultured in F-12 K medium containing 15.0 vol% heat-inactivated horse serum (Yuanyue Bio-Technology Co., Ltd, Shanghai) and 5.0 vol% heat-inactivated fetal bovine serum (Invigentech, Xi'an), under 5% CO₂ at 37 °C. The PC12 Cells were seeded in 96-well plates at a seeding density of 4×10^3 cells per well and allowed to adhere and grow. Once the cells reached the required confluence, they were placed into serum-containing medium and treated with various concentrations (0–200 μM) chelators L¹⁻³H or 100 μM H₂O₂ along with various concentrations (0–200 μM) chelators L¹⁻³H for 48 h, and then each cell was washed with PBS (Procell, Wuhan) three times. 100 μL of medium containing 10.0 vol CCK-8 (Invigentech, Xi'an) was directly added to each well and incubated for another 2 h under 5% CO₂ at 37 °C. The absorbance at 450 nm was detected by a microplate reader. The PC12 cells were cultured without test chelators or 100 μM H₂O₂ as a control group, and the results were expressed as the mean ± SD of three independent experiments by percentage of control.

Supplementary Information The online version contains supplementary material available at <https://doi.org/10.1007/s00775-021-01863-x>.

Acknowledgments The authors would like to thank Dr. Heyan Huang (Analytical and Testing Center, Southwest University of Science and Technology) for nuclear paramagnetic resonance measurements.

Author contributions QZ and RP conceived and designed the experiments; QZ, SF and YZ performed the experiments; QZ, and BJ analyzed the data; QZ and RP wrote and edited the manuscript.

Funding The research was funded by the National Natural Science Foundation of China (grant number 51972278), the Project of State Key Laboratory of Environment-friendly Energy Materials, Southwest University of Science and Technology (grant number 19fksy04), and the Natural Science Foundation of Southwest University of Science and Technology (grant number 18zx7136).

Declarations

Conflict of interest The authors declare that they have no conflict of interest.

References

- Zecca L, Youdim MB, Riederer P, Connor JR, Crichton RR (2004) Iron, brain ageing and neurodegenerative disorders. *Nat Rev Neurosci* 5(11):863–873. <https://doi.org/10.1038/nrn1537>
- Barnham KJ, Masters CL, Bush AI (2004) Neurodegenerative diseases and oxidative stress. *Nat Rev Drug Discov* 3(3):205–214. <https://doi.org/10.1038/nrd1330>
- Berg D, Gerlach M, Youdim MBH, Double KL, Zecca L, Riederer P, Becker G (2001) Brain iron pathways and their relevance to Parkinson's disease. *J Neurochem* 79(2):225–236. <https://doi.org/10.1046/j.1471-4159.2001.00608.x>
- Sun Y, Pham AN, Waite TD (2016) Elucidation of the interplay between Fe(II), Fe(III), and dopamine with relevance to iron solubilization and reactive oxygen species generation by catecholamines. *J Neurochem* 137(6):955–968. <https://doi.org/10.1111/jnc.13615>
- Sun Y, Pham AN, Waite TD (2018) Mechanism underlying the effectiveness of deferiprone in alleviating Parkinson's disease symptoms. *ACS Chem Neurosci* 9(5):1118–1127. <https://doi.org/10.1021/acscchemneuro.7b00478>
- Ward RJ, Dexter DT, Crichton RR (2015) Neurodegenerative diseases and therapeutic strategies using iron chelators. *J Trace Elem Med Biol* 31:267–273. <https://doi.org/10.1016/j.jtemb.2014.12.012>
- Kaur D, Andersen JK (2002) Ironing out Parkinson's disease: is therapeutic treatment with iron chelators a real possibility? *Aging Cell* 1(1):17–21. <https://doi.org/10.1046/j.1474-9728.2002.00001.x>
- Boddaert N, Le Quan Sang KH, Rötig A, Leroy-Willig A, Gallet S, Brunelle F, Sidi D, Thalabard J-C, Munnich A, Cabantchik ZI (2007) Selective iron chelation in Friedreich ataxia: biologic and clinical implications. *Blood* 110(1):401–408. <https://doi.org/10.1182/blood-2006-12-065433>
- Bolognin S, Drago D, Messori L, Zatta P (2009) Chelation therapy for neurodegenerative diseases. *Med Res Rev* 29(4):547–570. <https://doi.org/10.1002/med.20148>
- Pardridge WM (2007) Blood–brain barrier delivery. *Drug Discovery Today* 12(1):54–61. <https://doi.org/10.1016/j.drudis.2006.10.013>
- Tosato M, Marco VD (2019) Metal chelation therapy and Parkinson's disease: a critical review on the thermodynamics of complex formation between relevant metal ions and promising or established drugs. *Biomolecules* 9(7):269. <https://doi.org/10.3390/biom9070269>
- Lipinski CA, Lombardo F, Dominy BW, Feeney PJ (1997) Experimental and computational approaches to estimate solubility and permeability in drug discovery and development settings. *Adv Drug Deliv Rev* 23(1):3–25. [https://doi.org/10.1016/S0169-409X\(96\)00423-1](https://doi.org/10.1016/S0169-409X(96)00423-1)
- Ghose AK, Viswanadhan VN, Wendoloski JJ (1999) A knowledge-based approach in designing combinatorial or medicinal chemistry libraries for drug discovery. 1. A qualitative and quantitative characterization of known drug databases. *J Comb Chem* 1(1):55–68. <https://doi.org/10.1021/cc9800071>
- Pardridge WM (2001) Brain drug targeting: the future of brain drug development. Cambridge University Press, Cambridge
- Martin-Bastida A, Ward RJ, Newbould R, Piccini P, Sharp D, Kabba C, Patel MC, Spino M, Connelly J, Trieta F, Crichton RR, Dexter DT (2017) Brain iron chelation by deferiprone in a phase 2 randomised double-blinded placebo controlled clinical trial in Parkinson's disease. *Sci Rep* 7(1):1398. <https://doi.org/10.1038/s41598-017-01402-2>
- Singh S, Epemolu RO, Dobbin PS, Tilbrook GS, Ellis BL, Damani LA, Hider RC (1992) Urinary metabolic profiles in human and rat of 1,2-dimethyl- and 1,2-diethyl-substituted 3-hydroxypyridin-4-ones. *Drug Metab Dispos* 20(2):256–261
- Huang X-P, Spino M, Thiessen JJ (2006) Transport kinetics of iron chelators and their chelates in caco-2 cells. *Pharm Res* 23(2):280–290. <https://doi.org/10.1007/s11095-005-9258-5>
- Ma YM, Hider RC (2010) Design and synthesis of fluorine-substituted 3-hydroxypyridin-4-ones. *Tetrahedron Lett* 51(40):5230–5233. <https://doi.org/10.1016/j.tetlet.2010.07.134>

19. Ma Y, Kong X, Chen Y-L, Hider RC (2014) Synthesis and characterizations of pyridazine-based iron chelators. *Dalton Trans* 43(45):17120–17128. <https://doi.org/10.1039/C4DT02687J>
20. Ma Y, Xie Y, Hider RC (2013) A novel fluorescence method for determination of pFe³⁺. *Analyst* 138(1):96–99. <https://doi.org/10.1039/C2AN36186H>
21. Xie YY, Lu Z, Kong XL, Zhou T, Bansal S, Hider R (2016) Systematic comparison of the mono-, dimethyl- and trimethyl 3-hydroxy-4(1*H*)-pyridones—attempted optimization of the orally active iron chelator, deferiprone. *Eur J Med Chem* 115:132–140. <https://doi.org/10.1016/j.ejmech.2016.03.014>
22. Santos MA, Marques SM, Chaves S (2012) Hydroxypyridinones as “privileged” chelating structures for the design of medicinal drugs. *Coord Chem Rev* 256(1):240–259. <https://doi.org/10.1016/j.ccr.2011.08.008>
23. Santos MA, Chaves S (2015) 3-hydroxypyridinone derivatives as metal-sequestering agents for therapeutic use. *Future Med Chem* 7(3):383–410. <https://doi.org/10.4155/fmc.14.162>
24. Chand K, Rajeshwari R, Candeias E, Cardoso SM, Chaves S, Santos MA (2018) Tacrine–deferiprone hybrids as multi-target-directed metal chelators against Alzheimer’s disease: a two-in-one drug. *Metallomics* 10(10):1460–1475. <https://doi.org/10.1039/C8MT00143J>
25. Guillemette C (2003) Pharmacogenomics of human UDP-glucuronosyltransferase enzymes. *Pharmacogenomics J* 3(3):136–158. <https://doi.org/10.1038/sj.tpj.6500171>
26. Santos MA, Gama S, Gano L, Cantinho G, Farkas E (2004) A new bis(3-hydroxy-4-pyridinone)-IDA derivative as a potential therapeutic chelating agent. Synthesis, metal-complexation and biological assays. *Dalton trans* 21:3772–3781. <https://doi.org/10.1039/B409357G>
27. Gans P, Sabatini A, Vacca A (1999) Determination of equilibrium constants from spectrophotometric data obtained from solutions of known pH: the program pHab. *Anal Chim* 89(1–2):45–49. <https://doi.org/10.1109/TKDE.2004.1277824>
28. Alderighi L, Gans P, Ienco A, Peters D, Sabatini A, Vacca A (1999) Hyperquad simulation and speciation (HySS): a utility program for the investigation of equilibria involving soluble and partially soluble species. *Coord Chem Rev* 184(1):311–318. [https://doi.org/10.1016/S0010-8545\(98\)00260-4](https://doi.org/10.1016/S0010-8545(98)00260-4)
29. Gans P, Sabatini A, Vacca A (1996) Investigation of equilibria in solution. Determination of equilibrium constants with the HYPERQUAD suite of programs. *Talanta* 43(10):1739–1753. [https://doi.org/10.1016/0039-9140\(96\)01958-3](https://doi.org/10.1016/0039-9140(96)01958-3)
30. Nurchi VM, Crisponi G, Pivetta T, Donatoni M, Remelli M (2008) Potentiometric, spectrophotometric and calorimetric study on iron(III) and copper(II) complexes with 1,2-dimethyl-3-hydroxy-4-pyridinone. *J Inorg Biochem* 102(4):684–692. <https://doi.org/10.1016/j.jinorgbio.2007.10.012>
31. Chaves S, Delgado R, Da Silva JJRF (1992) The stability of the metal complexes of cyclic tetra-aza tetra-acetic acids. *Talanta* 39(3):249–254. [https://doi.org/10.1016/0039-9140\(92\)80028-C](https://doi.org/10.1016/0039-9140(92)80028-C)
32. Duffield JR, May PM, Williams DR (1984) Computer simulation of metal ion equilibria in biofluids. IV. plutonium speciation in human blood plasma and chelation therapy using polyaminopolycarboxylic acids. *J Inorg Biochem* 20(3):199–214. [https://doi.org/10.1016/0162-0134\(84\)85019-9](https://doi.org/10.1016/0162-0134(84)85019-9)
33. Kullgren B, Jarvis EE, An DD, Abergel RJ (2013) Actinide chelation: biodistribution and in vivo complex stability of the targeted metal ions. *Toxicol Mech Methods* 23(1):18–26. <https://doi.org/10.3109/15376516.2012.728641>
34. Wang X, Wu S, Guan J, Chen L, Shi C, Wan J, Liu Y, Diwu J, Wang J, Wang S (2019) 3-hydroxy-2-pyrrolidinone as a potential bidentate ligand for in vivo chelation of uranyl with low cytotoxicity and moderate decorporation efficacy: a solution thermodynamics, structural chemistry, and in vivo uranyl removal survey. *Inorg Chem* 58(5):3349–3354. <https://doi.org/10.1021/acs.inorgchem.8b03442>
35. Wang X, Dai X, Shi C, Wan J, Silver MA, Zhang L, Chen L, Yi X, Chen B, Zhang D, Yang K, Diwu J, Wang J, Xu Y, Zhou R, Chai Z, Wang S (2019) A 3,2-hydroxypyridinone-based decorporation agent that removes uranium from bones in vivo. *Nat Commun* 10(1):2570. <https://doi.org/10.1038/s41467-019-10276-z>
36. Blois MS (1958) Antioxidant determinations by the use of a stable free radical. *Nature* 181(4617):1199–1200. <https://doi.org/10.1038/1811199a0>
37. Pyrzynska K, Pękal A (2013) Application of free radical diphenylpicrylhydrazyl (DPPH) to estimate the antioxidant capacity of food samples. *Anal Methods* 5(17):4288–4295. <https://doi.org/10.1039/C3AY40367J>
38. Romano CS, Abadi K, Repetto V, Vojnov AA, Moreno S (2009) Synergistic antioxidant and antibacterial activity of rosemary plus butylated derivatives. *Food Chem* 115(2):456–461. <https://doi.org/10.1016/j.foodchem.2008.12.029>
39. Sharma OP, Bhat TK (2009) DPPH antioxidant assay revisited. *Food Chem* 113(4):1202–1205. <https://doi.org/10.1016/j.foodchem.2008.08.008>
40. Mishra K, Ojha H, Chaudhury NK (2012) Estimation of anti-radical properties of antioxidants using DPPH assay: a critical review and results. *Food Chem* 130(4):1036–1043. <https://doi.org/10.1016/j.foodchem.2011.07.127>
41. Foti MC, Daquino C, Geraci C (2004) Electron-transfer reaction of cinnamic acids and their methyl esters with the DPPH(*) radical in alcoholic solutions. *J Org Chem* 69(7):2309–2314. <https://doi.org/10.1021/jo035758q>
42. Cuvelier ME, Richard H, Berset C (1992) Comparison of the antioxidative activity of some acid-phenols: structure-activity relationship. *Biosci Biotechnol Biochem* 56(2):324–325. <https://doi.org/10.1271/bbb.56.324>
43. Shahidi F, Wanasundara PK (1992) Phenolic antioxidants. *Crit Rev Food Sci Nutr* 32(1):67–103. https://doi.org/10.1007/978-1-4899-1837-6_4
44. Sánchez-Moreno C, Larrauri JA, Saura-Calixto F (1998) A procedure to measure the antiradical efficiency of polyphenols. *J Sci Food Agric* 76(2):270–276. [https://doi.org/10.1002/\(SICI\)1097-0010\(199802\)76:2<3c270::AID-JSFA945%3e3.0.CO;2-9](https://doi.org/10.1002/(SICI)1097-0010(199802)76:2<3c270::AID-JSFA945%3e3.0.CO;2-9)
45. Hasegawa M, Ogihara T, Tamai H, Hiroi M (2009) Hypothermic inhibition of apoptotic pathways for combined neurotoxicity of iron and ascorbic acid in differentiated PC12 cells: reduction of oxidative stress and maintenance of the glutathione redox state. *Brain Res* 1283:1–13. <https://doi.org/10.1016/j.brainres.2009.06.016>
46. Rai BL, Dekhordi LS, Khodr H, Jin Y, Liu Z, Hider RC (1998) Synthesis, physicochemical properties, and evaluation of N-substituted-2-alkyl-3-hydroxy-4(1*H*)-pyridinones. *J Med Chem* 41(18):3347–3359. <https://doi.org/10.1021/jm9707784>

Publisher’s Note Springer Nature remains neutral with regard to jurisdictional claims in published maps and institutional affiliations.

Authors and Affiliations

Qingchun Zhang¹  · Shufan Feng¹ · Yulian Zhao² · Bo Jin¹ · Rufang Peng¹

✉ Qingchun Zhang
zhangqingchun@swust.edu.cn

✉ Rufang Peng
pengrufang@swust.edu.cn

² School of Life Science and Engineering, Southwest University of Science and Technology, Mianyang 621010, China

¹ State Key Laboratory of Environment-Friendly Energy Materials, School of Materials Science and Engineering, Southwest University of Science and Technology, Mianyang 621010, China